Mass Flow Rate Control in a Cylindrical Capillary by an AC Electric Field at High Zeta Potential

Prakash Goswami[1] and Suman Chakraborty[1,2,*]
[1]Department of Mechanical Engineering, Indian Institute of Technology Kharagpur, India 721302
[2]Advanced Technology Development Center, Indian Institute of Technology Kharagpur, India 721302

ABSTRACT
In the present study we obtain the mass flow rate characteristics in a cylindrical capillary due to a time-periodic electric field at high zeta potential, extending the conventional thin electrical double layer limit. The capillary cross section is divided into two regimes, the high potential regime (near surface region), and the low potential regime (capillary central line region). To obtain the potential distribution inside the capillary, the nonlinear part of the Poisson-Boltzmann equation is approximated by a linear function for the low potential regime and by an exponential function for high potential regime. Using the approximated potential distributions, the governing electro-hydrodynamic equation is then solved semi-analytically, where the imposed electric field and the velocity field is assumed to have the form which consist of a steady state term and a time-periodic term. A theoretical investigation on the mass flow rate, the phase difference is carried out on the basis of pulsation frequency, electric double layer thickness and the relative capillary radius. Moreover, this study is extended for triangular and trapezoidal shaped pulsation of the electric field. From the signature characteristics of the mass flow rate and the electric field, the "inverse" problem is also solved, that is, the desired electric field is obtained from a given mass flow rate.

1. INTRODUCTION

AC electroosmosis is the movement of an electrolyte solution in reference to a stationary charged surface under the application of a time-periodic or alternating electric field. Electroosmotic flows with time-periodic or ac electric field is primarily meant for abating the Joule heating effect in transport of thermally labile biological samples. In micro- and nano-scale transport process, the devices with moving parts (example: micro-stirrer) are difficult to fabricate and are very prone to mechanical failure. Moreover, the small diffusion length scale and negligible inertial effect makes it difficult for the device to reach efficient mixing of the samples or separate the species from a mixture. To overcome such difficulties, the microfluidic flow actuation mechanism using low strength ac electric field has found potential application in the field of biotechnology, separation science, microscale combustion and micromixers [1-6]. Apart from the experimental study, Dutta and Beskok [7] first reported ac electroosmotic flow theoretically. In their study, they derived an analytical model for time-periodic electroosmotic flow and gave an analogy similar to Stokes' second problem. Later on, the ac electroosmotic flows in rectangular and cylindrical microchannels has been studied by many researchers [8-19]. Reppert and Morgan [8] theoretically studied ac electroosmosis in cylindrical microcapillary which is based on the negligible inertial effect near the channel wall and a slip velocity consideration at the bulk. Kang et al. [9] used a Green's function approach to solve the complete

*Corresponding author: suman@mech.iitkgp.ernet.in

Poisson-Boltzmann equation for ac electroosmosis without considering the Debye-Hückel linearization. The fully developed laminar electrokinetic flow subjected to a sinusoidal driving force has been carried out by Bhattacharyya et al. [10]. Subsequently, these studies have been extended to rectangular geometry [11-12] and closed end rectangular and circular microchannels [13-14] which reveals distinctive nature of the electroosmosis due to the induced counterflow. Further, the ac electroosmotic flow through different geometrical conditions [15-17] and the consequences of overlapped electrical double layer effect [18-19] have also been reported in some literature.

The above literature is mainly focused on obtaining a desired velocity profile through the implication of an electric field, which has been represented in the form of a Fourier series. But it is interesting to note that, in microfluidic devices, the transport mechanism is mostly controlled by employing a mass flow rate rather than an imposed electroosmotic velocity field. Moreover, the "inverse" problem, that is, the determination of an unknown electric field which causes the required mass flow rate variation may have important technological consequences [20]. Chakraborty and Ray [21] reported this type of study for circular microchannels. In their study, they considered an electric field which consists of a steady part and a time varying perturbed part for obtaining the desired mass flow rate. Further, it has been extended to different nature of the electric field pulsation (such as triangular and trapezoidal pulsation). Obtaining the nature of the mass flow rate, they used it for studying the "inverse" problem. An expression for the unknown electric field has been obtained in terms of the amplitude and phase difference of the mass flow rate prediction. The above study is based on the consideration of Debye-Hückel linearization of Poisson-Boltzmann equation for potential distribution inside the capillary which is true for low values of the zeta potential. In a very recent study, Moghadam [22] also followed the same assumption and gave an exact solution for ac electroosmotic flow in cylindrical capillary using Green's function method. In this paper, we study the ac electroosmotic flow through a cylindrical microcapillary considering high zeta potential at the surface. A semi-analytical formalism is followed to obtain the mass flow rate assuming a sinusoidal electric field perturbation in addition to its steady base state. To determine the potential distribution, the Poisson-Boltzmann equation is solved approximately by dividing the whole regime into two regions, a high potential region and a low potential region [24].We also extend our study for triangular and trapezoidal type imposed field pulsation and the corresponding "inverse" problem.

2. MATHEMATICAL FORMULATION

2.1. Governing electro-hydrodynamic equations

We consider a cylindrical microcapillary of radius 'a'. A unidirectional flow is created by the application of an external ac electric field E_z along the longitudinal direction of the tube. Considering ρ to be the density and μ to be the dynamic viscosity of the fluid, the reduced form of the governing electro-hydro-dynamic equation in the cylindrical polar coordinate system is given by

$$\rho \frac{\partial u}{\partial t} = \mu \nabla^2 \left(u - \frac{\varepsilon E_z}{\mu} \psi \right) \tag{1}$$

where u is the longitudinal velocity, ε is the permittivity and ψ is the potential distribution (described in the sub-section 2.2) arises due to the ionic adsorption at the tube wall on the presence of a polar solvent. Assuming that, initially the fluid is at rest and it obeys the no-slip boundary condition at the wall, the pertinent initial and boundary conditions are

$$u = 0 \quad \text{at } t = 0 \quad \text{for all } r \tag{2a}$$

and for any finite time $t > 0$

$$u = 0 \quad \text{at } r = a \tag{2b}$$

and

$$\frac{\partial u}{\partial r} = 0 \quad \text{at } r = 0 \tag{2c}$$

We also assume the form of the applied electric field as

$$E_z = E_0 + \mathrm{Re}\left\{\sum_{n=1}^{\infty} E_n e^{i\omega_n t}\right\} \tag{3}$$

where E_0 is the steady component of the electric field, $\omega_n (= 2\pi nf)$ is the applied field frequency and $E_n = E_{cn} - iE_{sn}$ is the complex magnitude.

Analogously, the velocity field can be assumed as

$$u_e = u_{e0} + \mathrm{Re}\left\{\sum_{n=1}^{\infty} u_{en} e^{i\omega_n t}\right\} \tag{4}$$

where $u_e = u - \dfrac{\varepsilon E_z}{\mu}\psi$ is the velocity in reference to the electric field driven velocity.

Substituting (3) and (4) in the momentum equation (1), then computing the like powers of $e^{i\omega_n t}$, we get the differential equation for steady part and the time periodic part of the velocity as

$$\nabla^2 u_{e0} = 0 \tag{5a}$$

$$\nabla^2 u_{en} = \frac{i\omega_n \rho}{\mu}\left(u_{en} + \frac{\varepsilon E_n}{\mu}\psi\right) \tag{5b}$$

Using the non-dimensional variables $R = \kappa r$, $\Psi = ez\psi / k_B T$, $\bar{u}_{en} = u_{en} / u_0$, $\bar{E}_n = E_n / E_0$, the above equations (5a, b) can be reduced in the form

$$\frac{1}{R}\frac{d}{dR}\left(R\frac{d\bar{u}_{e0}}{dR}\right) = 0 \tag{6a}$$

$$\frac{1}{R}\frac{d}{dR}\left(R\frac{d\bar{u}_{en}}{dR}\right) = i\Omega_n \bar{u}_{en} + i\Omega_n \bar{E}_n \Psi \tag{6b}$$

where $\Omega_n = \dfrac{\omega_n \rho}{\mu\kappa^2}$ is the non-dimensional frequency and $u_0 = \dfrac{\varepsilon k_B T}{ez\mu}E_0$ is a characteristic velocity scale. Accordingly, the boundary conditions (2a, b) are also reduced in the form

$$\frac{d\bar{u}_{e0}}{dR} = 0,\ \frac{d\bar{u}_{en}}{dR} = 0 \quad \text{at } R = 0$$

and

$$\bar{u}_{e0} = -\bar{\xi},\ \bar{u}_{en} = -\bar{\xi}\,\bar{E}_n \quad \text{at } R = \kappa a$$

Solving the equations (6a,b) and using the above boundary conditions we have the velocity in the form

$$\overline{u} = \overline{u}_0 + \mathrm{Re}\left\{\sum_{n=1}^{\infty} \overline{u}_n e^{i\Omega_n \tau}\right\} \tag{7}$$

where $\tau = \dfrac{\mu\kappa^2}{\rho} t$ is the non-dimensional time-scale and

$$\overline{u}_0 = \left(\Psi - \overline{\xi}\right) \tag{8a}$$

$$\begin{aligned}\overline{u}_n = \overline{E}_n &\left(\Psi - \overline{\xi}\, \frac{I_0\left(R\sqrt{i\Omega_n}\right)}{I_0\left(\kappa a\sqrt{i\Omega_n}\right)} \right) - i\Omega_n \overline{E}_n I_0\left(R\sqrt{i\Omega_n}\right) \\ &\times \int_R^{\kappa a} \frac{1}{R I_0^2\left(R\sqrt{i\Omega_n}\right)} \left(\int_0^R R\Psi I_0\left(R\sqrt{i\Omega_n}\right) dR \right) dR\end{aligned} \tag{8b}$$

The mass flow rate at any instant of time across the tube cross section is obtained by integrating the mass of the fluid over the cross sectional area of the capillary and is given by

$$\dot{m} = 2\pi\rho \int_0^a r\, u(r,t)\, dr \tag{9}$$

which can be written in terms of the non-dimensional variables as

$$\dot{m} = \frac{2\pi\rho u_0}{\kappa^2} \left[\int_0^{\kappa a} R\,\overline{u}_0\, dR + \mathrm{Re}\left\{ \sum_{n=1}^{\infty} e^{i\Omega_n \tau} \int_0^{\kappa a} R\,\overline{u}_n\, dR \right\} \right] \tag{10}$$

Defining $\overline{u}_{avg} = \dfrac{2}{(\kappa a)^2} \displaystyle\int_0^{\kappa a} R\,\overline{u}_0\, dR$ and $\dot{\bar{m}} = \dfrac{\dot{m}}{\pi\rho a^2 u_0 \overline{u}_{avg}}$, from the above expression (10) we have the mass flow rate in the form

$$\dot{\bar{m}} = 1 + \mathrm{Re}\left\{ \sum_{n=1}^{\infty} \dot{\bar{m}}_n e^{i\Omega_n \tau} \right\}, \tag{11}$$

with $\dot{\bar{m}}_n = \dfrac{2}{(\kappa a)^2 \overline{u}_{avg}} \displaystyle\int_0^{\kappa a} R\,\overline{u}_n\, dR.$

Writing $\overline{E}_n = \left|\overline{E}_n\right| e^{i\theta_n}$, and $\phi_n = \dfrac{2e^{i\theta_n}}{(\kappa a)^2 \overline{u}_{avg} \left|\overline{E}_n\right|} \displaystyle\int_0^{\kappa a} R\,\overline{u}_n\, dR$, where $\left|\overline{E}_n\right|$, θ_n are the amplitude and argument of $\overline{E}_n$, respectively, the expression (11) can be recast in the form

$$\dot{\bar{m}} = 1 + \sum_{n=1}^{\infty} \left|\dot{\bar{m}}_n\right| \sin\left(\Omega_n \tau + \Delta\theta_n\right) \tag{12}$$

where $\left|\bar{\dot{m}}_n\right| = \left|\bar{E}_n\right|\left|\phi_n\right|$ represents the amplitude of the mass flow rate at n-th pulsation frequency and $\Delta\theta_n = \tan^{-1}\left\{\mathrm{Re}\left(\phi_n\right)/\mathrm{Im}\left(\phi_n\right)\right\}$ is the phase difference between the electric field and the mass flow rate.

Observing the equation (12) and the amplitude of the mass flow rate, it can be easily verified that, if any one of the mass flow rate or electric field is known, the other can be readily obtained. With this fact, here follows the "inverse" problem, that is, if the mass flow rate is given in the form

$$\bar{\dot{m}} = 1 + \sum_{n=1}^{\infty}\left|\bar{\dot{m}}_n\right|\sin\left(\Omega_n\tau\right), \tag{13}$$

one can readily obtain the electric field as

$$\bar{E}_z = 1 + \sum_{n=1}^{\infty}\left|\bar{E}_n\right|\sin\left(\Omega_n\tau - \Delta\theta_n\right), \tag{14}$$

where $\left|\bar{E}_n\right| = \left|\bar{\dot{m}}_n\right|/\left|\phi_n\right|$.

For a triangular pulsation, the mass flow rate $\bar{\dot{m}}$ can be written in the Fourier series form as [21]

$$\bar{\dot{m}} = 1 + \sum_{n=1}^{\infty}(-1)^{(n-1)}\frac{8\bar{\dot{m}}_A}{\pi^2(2n-1)^2}\sin\left(\Omega_{2n-1}\tau\right) \tag{15}$$

where as for a trapezoidal wave form it can be given by

$$\bar{\dot{m}} = 1 + \sum_{n=1}^{\infty}\frac{4\bar{\dot{m}}_A}{\pi^2 d}\frac{\sin((2n-1)\pi d)}{(2n-1)^2}\sin\left(\Omega_{2n-1}\tau\right) \tag{16}$$

where d is a fraction that characterizes the time of rise or fall in the wave form within $\tau = \pi$.

The Lanczos sigma factor is used for smoothening the rippling effects of Gibbs phenomena in the infinite sum of $\bar{\dot{m}}$ So the above mass flow rates for triangular and trapezoidal mass flow rates can be written in the form of a finite sum as [21]

$$\bar{\dot{m}} = 1 + \sum_{n=1}^{n_{\max}}\frac{8(-1)^{(n-1)}\bar{\dot{m}}_A}{\pi^2(2n-1)^2}\mathrm{sinc}\left(\frac{2(2n-1)}{2n_{\max}-1}\right)\sin\left(\Omega_{2n-1}\tau\right) \tag{17}$$

and

$$\bar{\dot{m}} = 1 + \sum_{n=1}^{n_{\max}}\frac{4\bar{\dot{m}}_A\sin((2n-1)\pi d)}{(2n-1)^2\pi^2 d}\mathrm{sinc}\left(\frac{2(2n-1)}{2n_{\max}-1}\right)\sin\left(\Omega_{2n-1}\tau\right) \tag{18}$$

respectively, where the 'sinc' function is defined by $\mathrm{sinc}(x) = \dfrac{\sin(x)}{x}$.

2.2. Potential distribution

The potential function ψ is effectively represents the electric double layer potential distribution. When the capillary is filled up with a polar solvent, the capillary surface acquires a net charge by the process of ionic adsorption or ionization of covalently bound surface groups present at the surface. This surface

charge is equal in magnitude and opposite in sign to that of the counterions present in the liquid. The monolayer of ions adjacent to the wall together with the diffuse layer is known as the electric double layer (EDL). This layer distributed over a length, commonly known as the Debye length, measured normally from the surface to a hypothetical distance at which the net charge decreases to 1/e of the surface potential. When the system is in equilibrium, for a symmetric binary fluid of valence z, the cation and anion concentration at the EDL is given by the Boltzmann distribution [23]

$$n^{\pm} = n_0 Exp\left[\mp\frac{ez\psi}{k_B T}\right] \tag{19}$$

where $n^{\pm}$ denotes the number density of cation and anion, n_0 is the bulk ionic concentration, e is the charge of a proton, k_B is the Boltzmann constant and T is the absolute temperature. Using equation (19) the net charge density in a unit volume of the fluid is given by

$$\rho_e = ez\left(n^+ - n^-\right) = -2n_0 ez\sinh\left(\frac{ez\psi}{k_B T}\right) \tag{20}$$

The relation between the EDL potential and the net volumetric charge density is given by the Poisson equation [23]

$$\nabla^2\psi = -\frac{\rho_e}{\varepsilon} \tag{21}$$

From equation (20) and (21), the differential equation for the potential distribution inside the cylindrical capillary is given by the Poisson-Boltzmann equation [23]

$$\frac{1}{r}\frac{d}{dr}\left(r\frac{d\psi}{dr}\right) = \frac{2n_0 ez}{\varepsilon}\sinh\left(\frac{ez\psi}{k_B T}\right) \tag{22}$$

Using the non-dimensional variables, $R = \kappa r$ and $\Psi = \frac{ez\psi}{k_B T}$, where κ $\left(= \sqrt{\frac{\varepsilon k_B T}{2n_0 e^2 z^2}}\right)$ is the reciprocal of the EDL thickness, the above equation can be written in the form

$$\frac{1}{R}\frac{d}{dR}\left(R\frac{d\Psi}{dR}\right) = \sinh(\Psi) \tag{23}$$

It is not possible to find an analytical solution for this equation. Here we follow the work of Levine et al. [24] to represent the potential distribution approximately, by solving equation (23). So representing the function sinh (Ψ) in the form [24]

$$\sinh(\Psi) = \begin{cases} \Psi & ;0 \le \Psi < 1 \\ \frac{1}{2}e^{\Psi} & ;1 < \Psi \le \bar{\xi} \end{cases}, \tag{24}$$

where $\bar{\xi}$ (= $ez\zeta/k_B T$) is the non-dimensional zeta potential, the above equation can be solved analytically within this two region.

If $\bar{\xi} \le 1$, then the potential distribution inside the cylindrical tube is given by

$$\Psi = \bar{\xi}\,\frac{I_0(R)}{I_0(\kappa a)} \tag{25}$$

where I_0 denotes the first order modified Bessel function of order zero.

If $\bar{\xi} > 1$, then the potential distribution inside the tube is solved for two region, the low potential region and high potential region, and is given by the differential equation

$$\frac{1}{R}\frac{d}{dR}\left(R\frac{d\Psi}{dR}\right) = \begin{cases} \Psi_L & ;0 \le R < R^* \\ \dfrac{1}{2}Exp\left[\Psi_H\right]; & R^* < R \le \kappa a \end{cases}, \tag{26}$$

where the subscripts *L* and *H* are used for the low and high potential regime of the tube, respectively. The boundary conditions are

$\left.\frac{d\Psi_L}{dR}\right|_{R=0} = 0$, $\Psi_H(\kappa a) = \bar{\xi}$, $\Psi_L(R^*) = \Psi_H(R^*) = 1$, and $\left.\frac{d\Psi_L}{dR}\right|_{R=R^*} = \left.\frac{d\Psi_H}{dR}\right|_{R=R^*}$,

where R^* is the tube radius at which $\Psi = 1$.

The solution for the potential distribution in the region $0 \le R < R^*$, is given by

$$\Psi_L = \frac{I_0(R)}{I_0(R^*)} \tag{27}$$

and in the region $R^* < R \le \kappa a$ is given by

$$\begin{aligned} \Psi_H &= \ln\left[\frac{c}{R^2}\left\{\tanh^2\left(-\frac{\sqrt{c}}{2}\left\{\ln(R)+A_+\right\}\right)-1\right\}\right] \quad \text{if } c>0 \\ &= \ln\left[-\frac{c}{R^2}\left\{\sec^2\left(\frac{\sqrt{-c}}{2}\left\{\ln(R)+A_-\right\}\right)\right\}\right] \quad \text{if } c<0 \\ &= -2\ln(R) - 2\ln\left(-\frac{1}{2}\left\{\ln(R)+A_0\right\}\right) \quad \text{if } c=0 \end{aligned} \tag{28}$$

where $c = \left(R^*\frac{I_1(R^*)}{I_0(R^*)}+2\right)^2 - eR^{*2}$, $A_0 = -\ln(R_0^*) - \frac{2}{R_0^*}e^{-1/2}$,

$$A_+ = -\ln(\kappa a) - \frac{2}{\sqrt{c}}\tanh^{-1}\sqrt{1+\frac{e^{\bar{\xi}}(\kappa a)^2}{c}} = -\ln(R^*) - \frac{2}{\sqrt{c}}\tanh^{-1}\sqrt{1+\frac{eR^{*2}}{c}}, \text{ and}$$

$$A_- = -\ln(\kappa a) + \frac{2}{\sqrt{-c}}\sec^{-1}\sqrt{\frac{e^{\bar{\xi}}(\kappa a)^2}{-c}} = -\ln(R^*) + \frac{2}{\sqrt{-c}}\sec^{-1}\sqrt{\frac{eR^{*2}}{-c}}$$

Here $R = R^*$ is the location at which $\Psi = 1$ and R_0^* is the position at which $c = 0$. The value of $c >$ or <0 will depend upon whether $R^* <$ or $> R_0^*$. If $c = 4$, then $R^* = 0$, which implies that the whole region of the tube will be high potential regime and in that case the potential distribution is given by

$$\Psi = \ln\left[\frac{4}{R^2}\left\{\tanh^2\left(-\left\{\ln(R)+A_H\right\}\right)-1\right\}\right] \tag{29}$$

where $A_H = -\ln(\kappa a) - \tanh^{-1}\sqrt{1+\frac{e^{\bar{\xi}}(\kappa a)^2}{4}}$.

3. RESULTS AND DISCUSSIONS

3.1. Velocity distributions

Although the results obtained in the previous sections are presented in the form of non-dimensional parameters, it is necessary to note the typical values of the dimensional parameters for practical consideration. For example, the typical value for density (ρ) and the kinematic viscosity (μ) of the fluid may be considered as $10^3 kg/m^3$ and $10^{-3} kg/ms$, respectively. For the electrochemical description, the parametric values may be considered as follows: $z = 1$ (for 1:1 electrolyte), $e = 1.6 \times 10^{-19} C$, T = 300$K$, $\varepsilon \approx 7.02 \times 10^{-10}\, C^2/m.J$, $k_B \approx 1.38 \times 10^{-23}\, J/K$. Figure 1 represents the variation in potential distribution across the capillary and the corresponding steady state electroosmotic velocity profile u_0 (due to the steady part of the electric field, i.e., E_0) for different values of the non-dimensional zeta potential($\bar{\xi}$) which are taken as 10, 20 and 30. The potential profile is plotted using the expressions given in equations (27), (28) and (29). From the typical behavior of the potential profile in Figure 1, it is evident that at high zeta potential the central line potential does not tends to zero as of the low values of zeta potential for a constant EDL thickness parameter K (= κa).

To account the effect of pulsating field frequency, the electroosmotic velocity under such circumstances are shown in Figure 2(a-c). Since, any kind of pulsating field can be represented in the form of a Fourier series, without loss of generality, the perturbed component of the electric field is taken as sinusoidal in nature. A single pulsation (i.e., $n = 1$ in the infinite sum of electric field pulsation) is considered to obtain the signature characteristic of the velocity field which is presented at some time instant (ranges from 0 to 2π), for various values of the non-dimensional EDL thickness parameter whereas the value of the non-dimensional zeta potential ($\bar{\xi}$) is kept at 20. The qualitative nature of the velocity profiles are same as reported in Chakraborty and Ray [21]. In the inset of each figure, the time periodic component of the velocity profile is shown. It is observed from the Figure 2(a-c) that, as the EDL thickness parameter K increases the electric field response to the velocity decreases. Since, the increase in K corresponds to the lower values of EDL thickness, the zeta potential decreases to its bulk

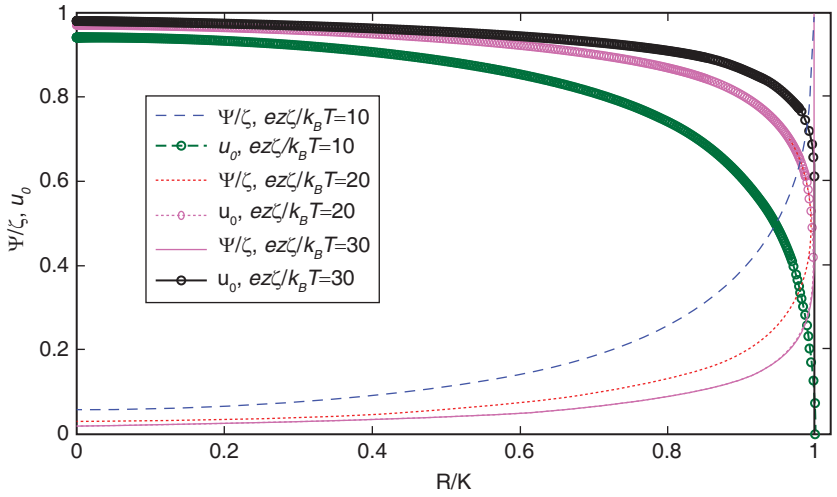

Figure 1. The potential distribution and the steady state electroosmotic velocity with respect to the channel radius for different values of the zeta potential

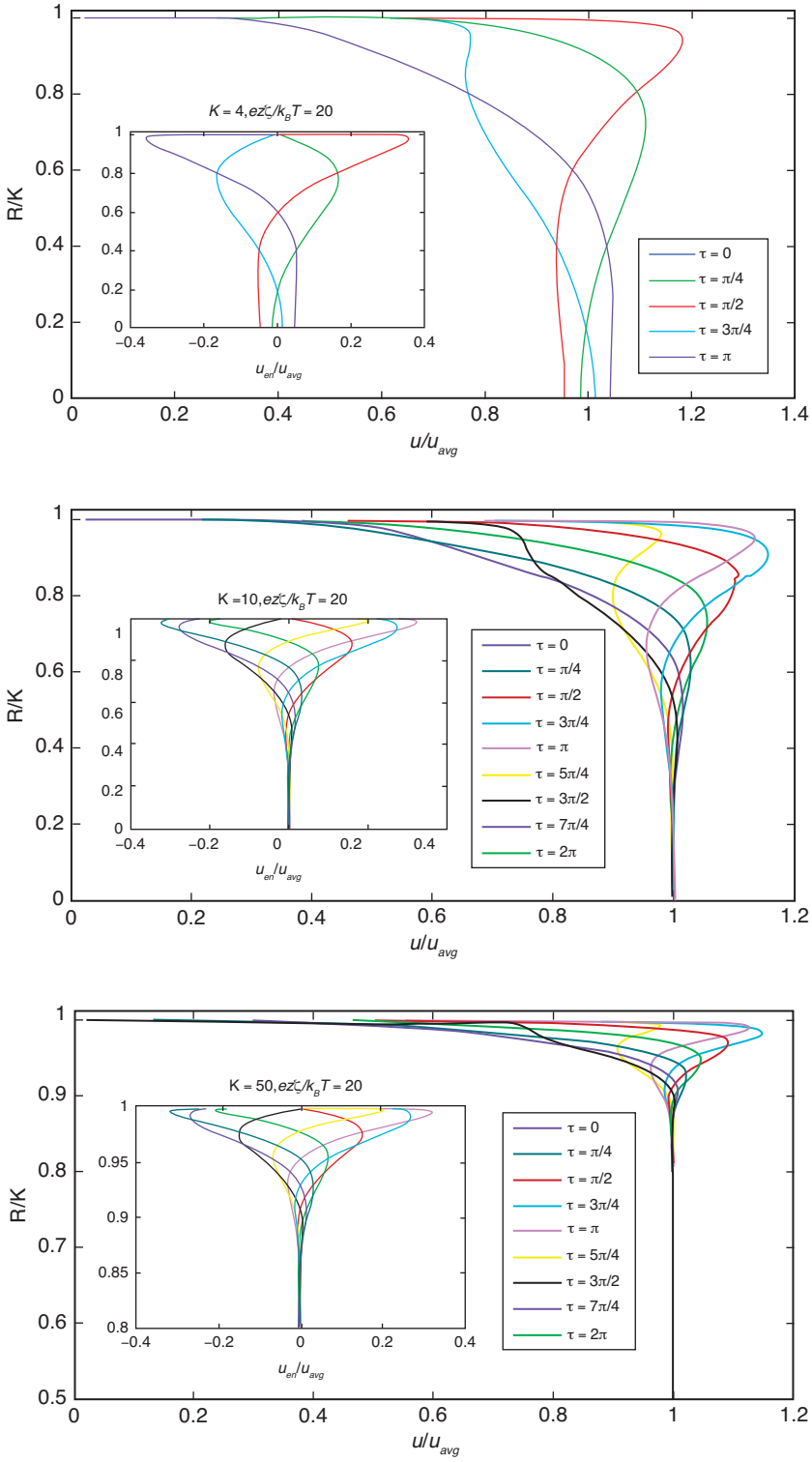

Figure 2(a-c). AC electroosmotic velocity profile across the capillary for $\bar{\zeta} = 20$, corresponding to the values of EDL thickness parameter(a) K = 4 (b) K = 10 (c) K = 50

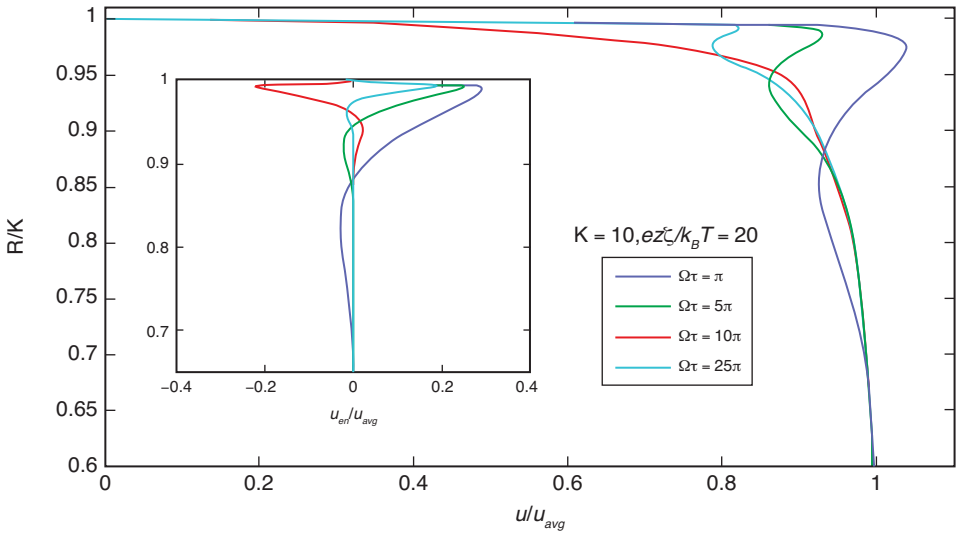

Figure 3. AC electroosmotic velocity profile for different values of the frequency parameter (Ω= 4, 20, 40, 100), taking K=10 and $\bar{\zeta} = 20$

value through a very small region adjacent to the capillary wall. So, the effect of the pulsation frequency on the diffuse layer of the EDL does not propagate into the bulk and as a result the bulk fluid remains unresponsive, which is shown in Figure 2(c), the case K = 50. But for a higher EDL thickness, i.e., Figure 2(a) where K = 4; due to the larger diffuse layer available for the potential distribution, the bulk fluid also responds to the excitation frequency.

The variation in imposed frequency Ω, on the velocity profile is shown in Figure 3. The expression for velocity profile given in equation (7) is plotted at a particular time ($\tau = \pi/4$) for different field frequency (Ω = 4, 20, 40, 100), keeping K and ζ constant. It is observed that as the field frequency increases, the periodic nature of the velocity profile inside the diffuse layer diminishes. At high frequency the imposed electric field changes its course very rapidly. Also, the increase in the value of Ω (which is the ratio of frequency ω to the diffusion time scale $\kappa^2 \nu$) corresponds to the larger diffusion time scale compared to the frequency time scale. As a result, the momentum does not get enough time to diffuse into the bulk.

3.2. Mass flow rate

The mass flow rate prediction, as obtained in equation (12), is depicted in Figure 4(a-b) with respect to time for a single ($n = 1$) sinusoidal pulsation on the imposed electric field. The amplitude and the phase lag of the mass flow rate is obtained from the expression $|\bar{m}_1| = |E_1||\phi_1|$ and $\Delta\theta_1 = \tan^{-1}\{\mathrm{Im}(\phi_1)/\mathrm{Re}(\phi_1)\}$, respectively. In Figure 4(a), the variation in the mass flow rate due to the EDL thickness parameter is illustrated. Here, the amplitude of the electric field and the non-dimensional zeta potential is considered as 0.5 and 20, respectively. For further illustration, in Figure 4(b), the variation in the zeta potential is considered whereas the EDL thickness parameter is fixed at 50. The mass flow rate increases as the EDL thickness increases. But in case of variation in the zeta potential, there does not have much variation in the mass flow rate because of the low value of the EDL thickness considered. A phase difference between the imposed electric field and the mass flow rate is observed. In an immediate study, after obtaining the amplitude ratio $|\phi_1|$, one may obtain the amplitude of the required electric field as

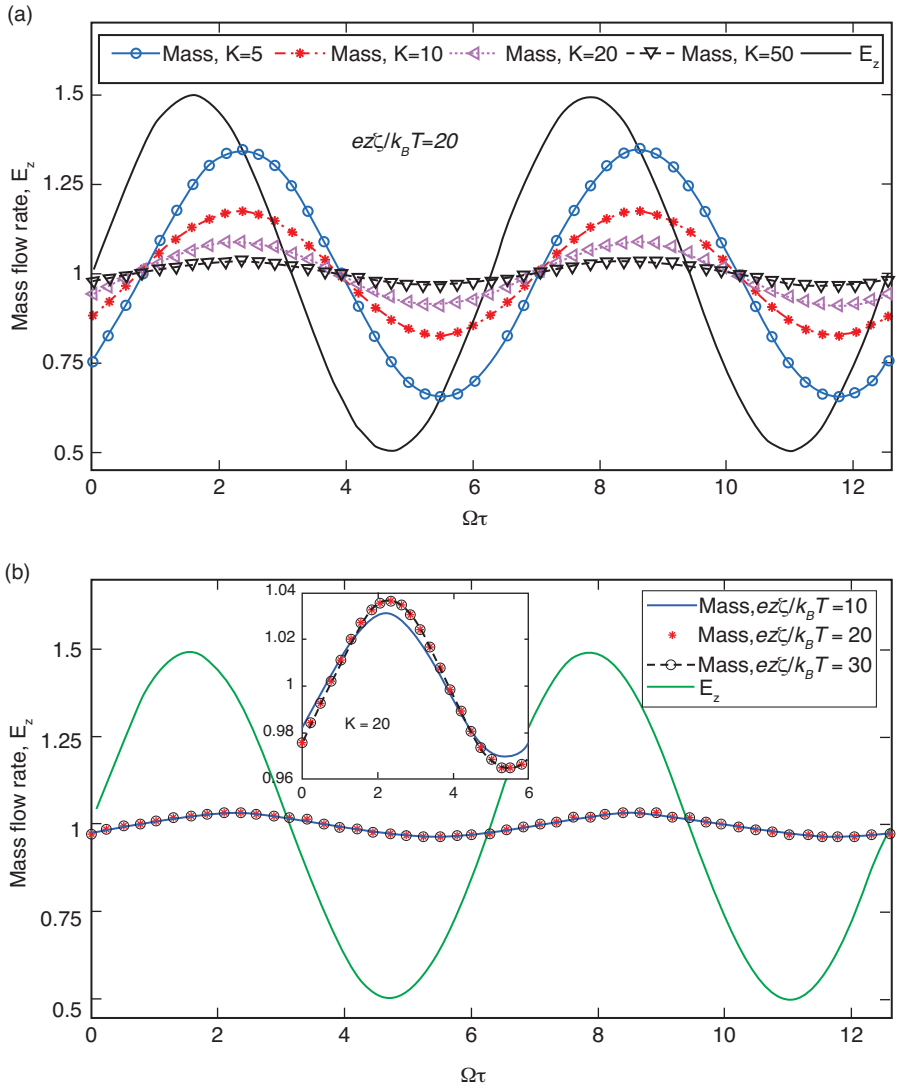

Figure 4(a). The mass flow rate for a given electric field for different non-dimensional EDL thickness (b). The mass flow rate for a given electric field for different non-dimensional zeta potential

$|E_1| = |\dot{\bar{m}}_1| / |\phi_1|$ and the phase lag as $-\Delta\theta_1$. Using these values in equation (14), the electric field is plotted in Figure 5(a-b), for different values of the EDL thickness parameter and non-dimensional zeta potential. It is observed from figure 5(a) that for a given mass flow rate, the required electric field becomes larger as the EDL thickness parameter increases. This happens because of the reduction in EDL thickness reduces the strength of the flow momentum significantly. So, to aggravate this momentum deficit a larger electric field is required to generate the same amount of volume flow rate, as compared to that of the higher EDL thickness. With this observation, a similar conclusion may be drawn for the zeta potential variation. That is, for a given mass flow rate the required electric field is larger for small zeta potential ($\bar{\zeta} = 10$) as compared to the large value of the zeta potential ($\bar{\zeta} = 30$),

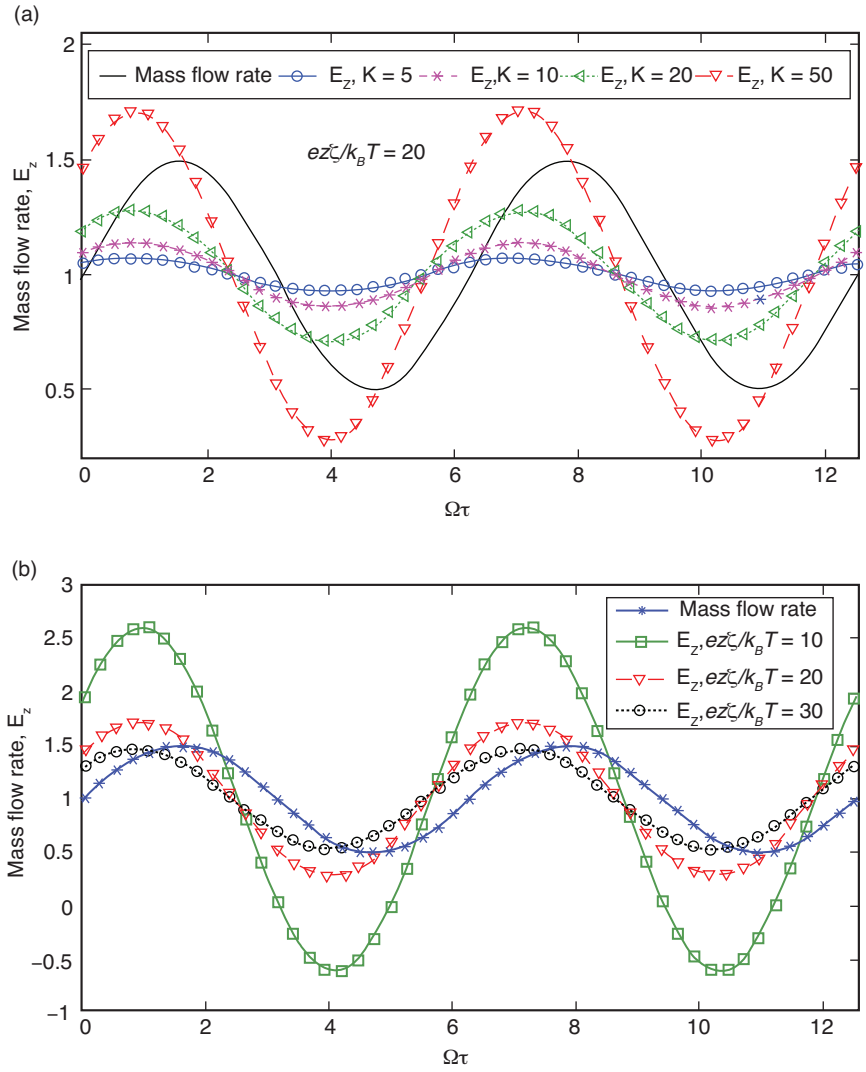

Figure 5(a). The required electric field for a given mass flow rate at different non-dimensional EDL thickness (b). The required electric field for a given mass flow rate at different non-dimensional zeta potential

which is evident from Figure 5(b). In this regard it is also important to note that the mass flow rate is positive over the entire transient regime, whereas the required electric field may be negative for some combination of the values of K, Ω and $\overline{\xi}$ (Figure 5(b)). This implies that the parameters representing EDL thickness, pulsation frequency and the zeta potential play important role in controlling the mass flow rate and as well as the required electric field.

Thus, we have outlined the mass flow rate prediction for a given sinusoidally perturbed electric field and its "inverse" consequence, that is, the required electric field for a desired mass flow rate. Let us consider the nature of the perturbed field as either triangular or trapezoidal. The Fourier series representation of such pulsation is given by expression (15) for triangular pulsation and (16) for trapezoidal pulsation. It is notable that, in the series representation only the odd harmonics of the excitation frequency are present in the infinite sum. For computational purpose it is necessary to

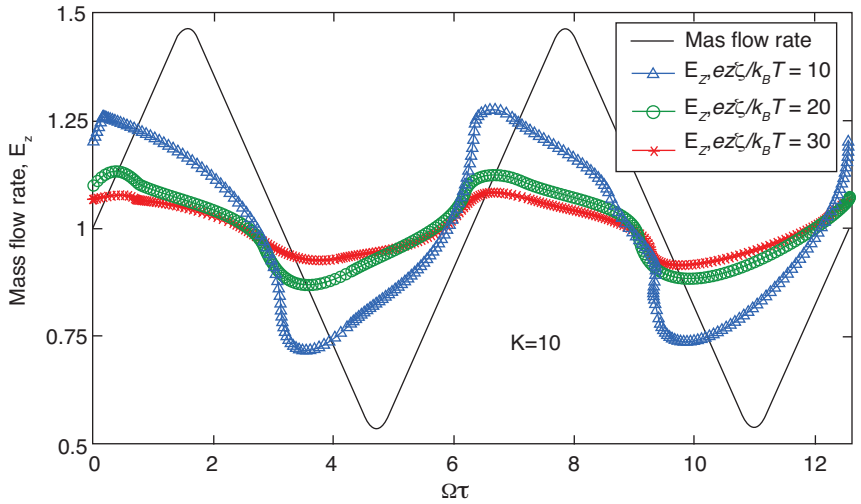

Figure 6(a). The electric field for a given mass flow rate at different non-dimensional zeta potential (triangular pulsation)

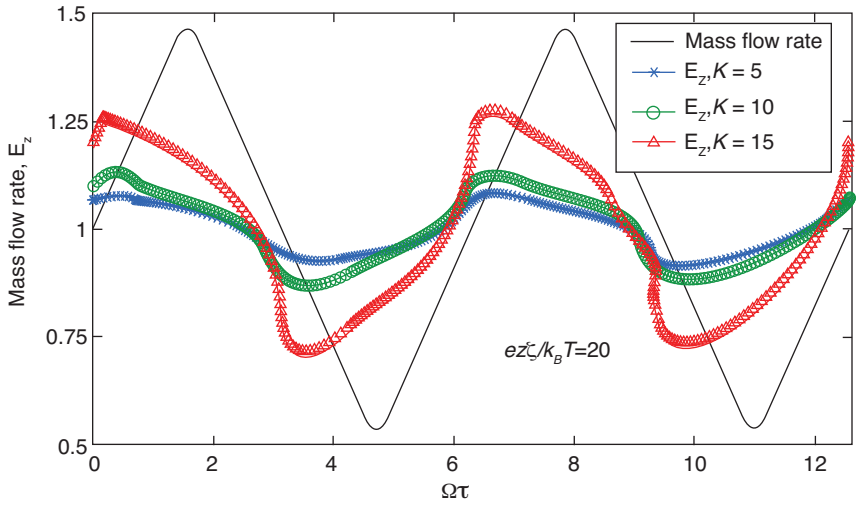

Figure 6(b). The electric field for a given mass flow rate at different non-dimensional edl thickness (triangular pulsation)

consider the truncated finite series of (15) and (16) and the upper limit of the sum is denoted by n_{max}. In computation of these finite Fourier series, it is inevitable to avoid the Gibbs phenomena in the form of rippling effects. A Lanczos sigma factor [21] of the form 'sinc $(2(2n-1))/(2n_{max}-1))^5$' is used to smoothening this rippling effect. The required electric field for generating triangular and trapezoidal type mass flow rate is shown in Figure 6(a-b) and 7(a-b), respectively. The electric field is plotted using equation (17) and (18) for triangular and trapezoidal pulsation, taking n_{max}=20. The parameters for trapezoidal pulsation is taken as $d = 0.1$, $\dot{\bar{m}}_A = 0.2$ and for the triangular pulsation $\dot{\bar{m}}_A = 0.5$. In figure 6(a) the variation in the zeta potential parameter is considered keeping K fixed, whereas in figure 6(b) the variation in the EDL thickness parameter considered keeping $\bar{\zeta}$ fixed. The variation in the required electric field due to the changes in the parameters follows the same behavior as of the sinusoidal pulsation, except some sharp distortion with respect to the time variable. From figure 6(a-b) and 7(a-b)

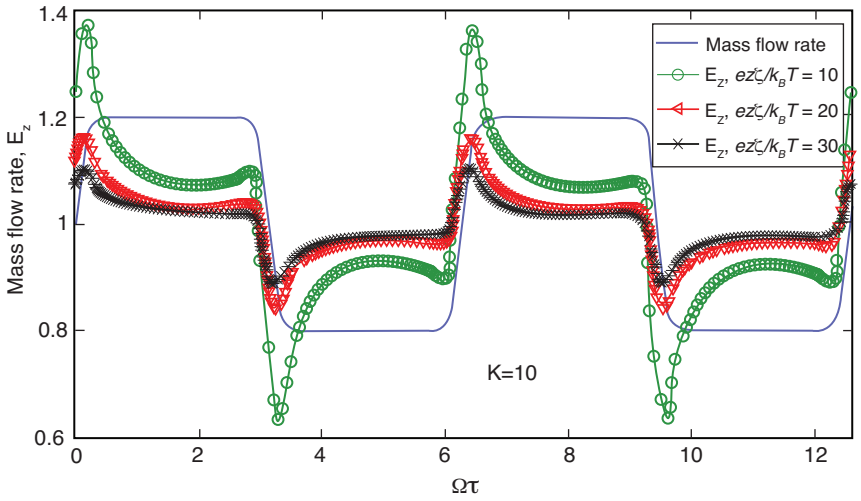

Figure 7(a). The electric field for a given mass flow rate at different non-dimensional zeta potential (trapezoidal pulsation)

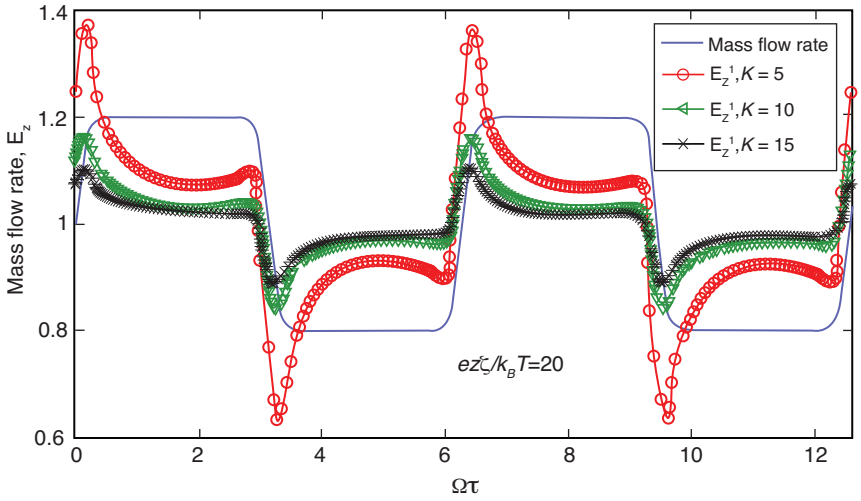

Figure 7(b). The electric field for a given mass flow rate at different non-dimensional EDL thickness (trapezoidal pulsation)

it is observed that these distortions are arises at the position where the nature of the pulsation is either rising or falling. So, at these junctions, the alteration in the flow momentum may give such distortion on the required electric field. From this study it can be concluded that, if the electric field is controlled in the manner shown in figure 6(a-b) and 7(a-b), one may obtain a mass flow rate of triangular or trapezoidal nature.

4. CONCLUSIONS

In this study, we have presented the mass flow rate control in a cylindrical capillary by an ac electric field through a semi-analytical formalism, considering high zeta potential at the capillary surface. The expression for the potential distribution as well as the velocity and mass flow rate has been obtained in terms of non-dimensional parameters. The amplitude of the mass flow rate has been presented as a product of electric field amplitude and the amplitude of the momentum flux across the tube cross

section. Initially, a signature characteristic for the mass flow rate has been obtained for sinusoidal electric field pulsation. The form of the required electric field for a desired mass flow rate pulsation has also been outlined. It has been observed from the study that the amplitude of the required electric field strongly depends on the excitation frequency, zeta potential and the EDL thickness. Keeping in mind that any periodic pulsation can be represented in a Fourier series, this study have been further extended to triangular and trapezoidal type field pulsation.

ACKNOWLEDGEMENTS

The author P. Goswami is thankful to ***National Board for Higher Mathematics, Department of Atomic Energy, INDIA*****,** for their financial support in the form of a research fellowship.

REFERENCES

[1] M. Minor, A.J. van der Linde, H.P. van Leeuwen, and J. Lyklema, Dynamic aspects of electrophoresis and electroosmosis: A new fast method for measuring particle mobilities, *Journal of Colloid and Interface Science*, **189**, 1997, 370.

[2] A. Ramos, H. Morgan, N. G. Green and A. Castellanos, Ac electrokinetics: A review of forces in microelectrode structures, *Journal of Physics D: Applied Physics,* **31**, 1998, 2338.

[3] A. Ramos, H. Morgan, N. G. Green and A. Castellanos, Ac electric-field-induced fluid flow in microelec-trodes, *Journal of Colloid and Interface Science*, **217**, 1999, 420.

[4] V. M. Barragan and C. R. Bauza, Electrosmosis through a cation exchange membrane: Effect of ac perturbation on the electroosmotic flow, *Journal of Colloid and Interface Science,* **230**, 2000, 359.

[5] A. B. D. Brown, C. G. Smith and A. R. Rennie, Pumping of water with ac electric fields applied to asymmetric pairs of microelectrodes, *Physical Review E*, **63**, 2001, 016305.

[6] V. Studeer, A. Pepin, Y. Chen, and A. Ajdari, Fabrication of microfluidic devices for AC electrokinetic fluid pumping, *Microelectronic Engineering,* **61**, 2002, 915.

[7] P. Dutta and A. Beskok, Analytical solution of time periodic electroosmotic flows: Analogies to Stokes' second problem, *Analytical Chemistry,* **73**, 2001, 5097.

[8] P. M. Reppert and F. D. Morgan, Frequency dependent electroosmosis, *Journal of Colloid and Interface Science*, **254**, 2002, 372.

[9] Y. J. Kang, C. Yang and X. Y. Huang, AC electroosmosis in microchannnels packed with a porous medium, *Journal of Micromechanics and Microengineering*, **14**, 2002, 1249.

[10] A. Bhattacharyya, J. H. Masliyah, and J. Yang, Oscillating laminar electrokinetic flow in infinitely extended circular microchannels, *Journal of Colloid and Interface Science*, **261**, 2003, 12.

[11] J. Yang, A. Bhattacharyya, J. H. Masliyah and D. Y. Kwok, Oscillating laminar electrokinetic flow in infinitely extended rectangular microchannels, *Journal of Colloid and Interface Science,* **261**, 2003, 21.

[12] D. Erickson and D. Li, Analysis of ac electroosmotic flows in a rectangular microchannel, *Langmuir*, **19**, 2003, 5421.

[13] Marcos, C. Yang, K. T. Ooi, T. N. Wong and J. H. Masliyah, Frequency-dependent laminar electroosmotic flow in a closed-end rectangular microchannel, *Journal of Colloid and Interface Science*, **275**, 2004, 679.

[14] Marcos, Y. J. Kang, K. T. Ooi, C. Yang and T. N. Wong, Frequency-dependent velocity and vorticity fields of electro-osmotic flow in a closed-end cylindrical microchannel, *Journal of Micromechanics and Microengineering*, **15**, 2005, 301.

[15] W. J. Luo, Y. J. Pan and R. J. Yang, Transient analysis of electro-osmotic secondary flow induced by dc or ac electric field in a curved rectangular microchannel, *Journal of Micromechanics and Microengineering*, **15**, 2005, 463.

[16] X. Xuan and D. Li, Electroosmotic flow in microchannels with arbitrary geometry and arbitrary distribution of wall charge, *Journal of Colloid and Interface Science*, **289**, 2005, 291.

[17] Y. J. Kang, C. Yang and X. Y. Huang, Dynamic aspects of electroosmotic flow in a cylindrical microcapillary, *International Journal of Engineering Sciences,* **40**, 2002, 2203.

[18] S. Chakraborty and A. K. Srivastava, A generalized model for time periodic electroosmotic flows with overlapping electrical double layers, *Langmuir,* **23**, 2007, 12421.

[19] S. Chakraborty and S. Talapatra, Double layer overlap in AC-electroosmosis, *European Journal Mechanics B/Fluids*, **27**, 2008, 297.

[20] S. Chakraborty and S. Padhy, Induced pressure gradients due to entrance and exit effects in electroosmotically driven flows through nanopores within the continuum regime, *Journal of Physics D: Applied Physics*, **41**, 2008, 065502.

[21] S. Chakraborty and S. Ray, Mass flow-rate control through time periodic electro-osmotic flows in circular microchannels, *Physics of Fluids*, **20**, 2008, 1.

[22] A. J. Moghadam, An exact solution of AC electro-kinetic-driven flow in a circular micro-channel, *European Journal Mechanics B/Fluids*, **34**, 2012, 91

[23] R. J. Hunter, *Zeta Potential in Colloid Sciences*, Academic Press, San Diego, 1981.

[24] S. Levine, J. R. Marriott, G. Neale and N. Epstein, Theory of electrokinetic flow in fine cylindrical capillaries at high zeta potentials, *Journal of Colloid and Interface Science*, **52**, 1975, 136.